

Driven-dissipative criticality within the discrete truncated Wigner approximation

Vijay Pal Singh^{1,2} and Hendrik Weimer¹

¹*Institut für Theoretische Physik, Leibniz Universität Hannover, Appelstraße 2, 30167 Hannover, Germany*

²*Zentrum für Optische Quantentechnologien and Institut für Laserphysik, Universität Hamburg, 22761 Hamburg, Germany*
(Dated: March 29, 2022)

We present an approach to the numerical simulation of open quantum many-body systems based on the semiclassical framework of the discrete truncated Wigner approximation. We establish a quantum jump formalism to integrate the quantum master equation describing the dynamics of the system, which we find to be exact in both the noninteracting limit and the limit where the system is described by classical rate equations. We apply our method to simulation of the paradigmatic dissipative Ising model, where we are able to capture the critical fluctuations of the system beyond the level of mean-field theory.

The identification of phase transitions and their universality classes is one of the most important tasks in many-body physics, especially for non-equilibrium systems where many of the conventional methods cannot be applied. Here, we show that a large class of steady state phase transitions arising in open quantum systems can be efficiently simulated and analyzed using an open system variant of the discrete truncated Wigner approximation.

Open quantum many-body systems are not only useful for the dissipative preparation of tailored quantum many-body states [1–12], but are also of fundamental interest, as their dynamics can realize non-equilibrium phenomena that are not found in their closed counterparts. Most strikingly, the steady state of an open system can undergo phase transitions [13–36], where an associated order parameter changes across the transition in a non-analytic way. A large class of such transitions is governed by a dynamical symmetry rendering static correlation functions to obey thermal statistics [37, 38]. Of particular interest is a dissipative variant of the Ising model in a transverse field [20] because of its relevance for ongoing experiments with driven-dissipative Rydberg gases [39, 40]. For this model, a first-order liquid-gas transition has been reported, which has been predicted to end in an Ising critical point based on mean-field calculations [41]. However, since the numerical analysis of critical open many-body systems is extremely challenging [42], a reliable assesment of its critical behavior is still lacking.

In this Letter, we build upon the discrete truncated Wigner approximation [43] and introduce a variant capable to treat open quantum systems. Our approach constitutes a wave function Monte-Carlo method in the quantum-jump formalism [44–46]. Crucially, our method is exact in the non-interacting limit, which we use for benchmarking, as well as in the fully classical limit, where coherences in the density matrix vanish and the dynamics is governed by classical rate equations. We then apply our method to the dissipative Ising model on a square lattice, where we find that the transition belongs to the two-dimensional Ising universality class. Remarkably, we obtain critical exponents beyond their mean-field value,

although the interaction is only taken into account on a mean-field level. We connect this surprising result to the fact that classical fluctuations are correctly taken into account, while quantum fluctuations are irrelevant at the transition. This scenario is characteristic for all open quantum systems possessing the aforementioned dynamical symmetry, hence our method can be expected to correctly describe the critical behavior of a large class of dissipative many-body models, e.g. the dissipative XYZ model [47].

Open-system discrete truncated Wigner approximation (OSDTWA).— Phase-space methods, such as the truncated Wigner approximation (TWA), approximate the quantum-mechanical dynamics by a semiclassical evolution of individual trajectories. In the TWA, which has also been employed to investigate open quantum systems [48–52], the initial state is sampled from a continuous Wigner function [53], which is replaced by a discrete Wigner functions for systems with discrete degrees of freedom [54]. For a single spin-1/2 particle, we represent the discrete phase space by four phase points $\alpha = (q, p) \in \{(0, 0), (0, 1), (1, 0), (1, 1)\}$ [43, 54, 55]. The corresponding phase-point operators \hat{A}_α are written in terms of the Pauli matrices $\hat{\sigma} = (\hat{\sigma}^x, \hat{\sigma}^y, \hat{\sigma}^z)$ as

$$\hat{A}_\alpha = \hat{\phi}(\mathbf{r}_\alpha), \quad \hat{\phi}(\mathbf{r}) \equiv (\hat{\sigma}^0 + \mathbf{r} \cdot \hat{\sigma})/2, \quad (1)$$

with the vectors $\mathbf{r}_{(0,0)} = (1, 1, 1)$, $\mathbf{r}_{(0,1)} = (-1, -1, 1)$, $\mathbf{r}_{(1,0)} = (1, -1, -1)$, and $\mathbf{r}_{(1,1)} = (-1, 1, -1)$ [54]. Note that we have also included a $\hat{\sigma}^0$ term to allow sampling from unnormalized density matrices. For a system with N spin-1/2 the phase space spans by 4^N points, i.e., $\alpha = \{\alpha_1, \alpha_2, \dots, \alpha_N\}$. The time evolution evolves under the classical dynamics of phase-space variables as

$$\langle \hat{O} \rangle(t) = \sum_{\alpha} w_{\alpha}(0) \mathcal{O}_{\alpha}^W(t) \approx \sum_{\alpha} w_{\alpha}(0) \mathcal{O}_{\alpha}^{W,cl}(t), \quad (2)$$

where \mathcal{O}_{α}^W is the Weyl symbol for the operator \hat{O} and $\mathcal{O}_{\alpha}^{W,cl}(t)$ represents the classical evolution. $w_{\alpha}(0)$ is the initial Wigner function on the discrete many-body phase space. It factorizes for every spin i , i.e., $w_{\alpha}(0) = \prod_{i=1}^N w_{\alpha_i}^{[i]}$, where the superscript $[i]$ denotes the phase

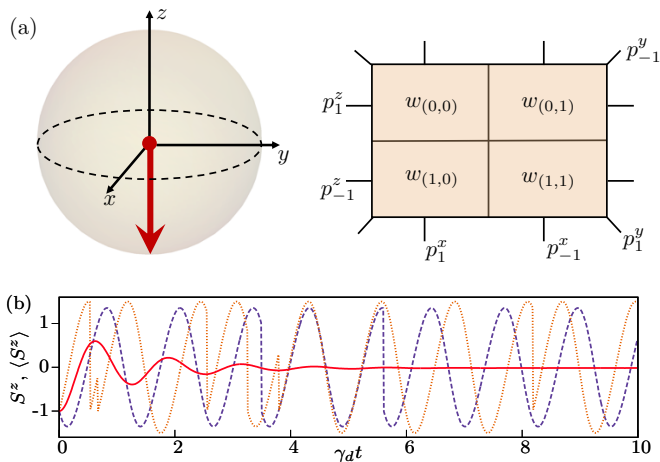


FIG. 1. Open-system dynamics within the discrete truncated Wigner approximation. (a) Bloch sphere representation for a spin-1/2 particle, where the spin points in the $-z$ direction. This initial state is sampled from a discrete four-point Wigner quasiprobability distribution $w_{(p,q)}$, which are $w_{(0,0)} = w_{(0,1)} = 0$ and $w_{(1,0)} = w_{(1,1)} = 1/2$. The probability for a spin to point along the $\pm x$, $\pm y$, and $\pm z$ directions ($p_{\pm 1}^{x,y,z}$) is given by the sum over the vertical, diagonal, and horizontal lines, respectively [43, 54]. (b) Classical trajectories corresponding to two different initial configurations (dotted and dashed lines) for single spin and $g/\gamma_d = 5$. The averaged time evolution of $\langle S^z(t) \rangle$ over 10^5 trajectories is shown as a continuous line.

space for spin i . Similarly, for the initial density matrix we have $\hat{\rho}(0) = \prod_{i=1}^N \hat{\rho}^{[i]}$. For the initial state with spins pointing in the $-z$ direction, $w_{\alpha_i}^{[i]} = \text{Tr}[\hat{\rho}^{[i]}(\hat{z})\hat{A}_{\alpha_i}]/2$ yields $w_{(0,0)}^{[i]} = w_{(0,1)}^{[i]} = 0$ and $w_{(1,0)}^{[i]} = w_{(1,1)}^{[i]} = 1/2$ for every spin i . This is illustrated in Fig. 1(a), where the three sets of lines (two horizontal, two vertical, and two diagonal) correspond to the probability of a measurement outcome. This means the probability for a spin being in the $+z$ and $-z$ direction is 0% and 100%, respectively. Similarly, the probabilities for a spin being in the $\pm x$ and $\pm y$ directions are 50% and 50%, respectively.

To solve the open-system dynamics we use the quantum master equation in Lindblad form

$$\frac{d}{dt}\hat{\rho} = -i[\hat{H}, \hat{\rho}] + \sum_i \left(\hat{c}_i \hat{\rho} \hat{c}_i^\dagger - \frac{1}{2} \{ \hat{c}_i^\dagger \hat{c}_i, \hat{\rho} \} \right), \quad (3)$$

where the Hamiltonian \hat{H} describes the coherent evolution and the jump operators \hat{c}_i correspond to the incoherent part of the dynamics. While our OSDTWA approach is completely generic, we will exemplify our method for a dissipative variant of the Ising model in a transverse field [20], which is one of the most important models in the analysis of open quantum many-body systems. The interest in this model does not only stem from the paradigmatic character similar to the transverse-field Ising model for closed quantum systems [56], but also from its importance to understand

experimental results obtained in strongly interacting Rydberg gases [39, 40]. Its Hamiltonian has the conventional form $\hat{H} = (g/2) \sum_i \hat{\sigma}_i^x + (V/4) \sum_{\langle ij \rangle} \hat{\sigma}_i^z \hat{\sigma}_j^z$, where g is the transverse field and V is the nearest-neighbor interaction. Dissipation is introduced via spin-flip operators $\hat{c}_i = \sqrt{\gamma_d} \hat{\sigma}_i^-$, with γ_d being the decay rate of the up spins and $\hat{\sigma}_i^- = (\hat{\sigma}_i^x - i\hat{\sigma}_i^y)/2$. This model can be realized using laser-driven Rydberg atoms, for which the spin-down state corresponds to the atomic ground state and the spin-up state refers to an excited Rydberg state. Transitions between the states are driven by a coherent laser with a Rabi frequency $\Omega = g$ and the interaction V describes a repulsive van der Waals interaction C_6/a^6 determined by a C_6 coefficient at the lattice spacing a [57].

In the following, we obtain the dynamics of the interacting many-body system by replacing the time evolution via classical trajectories as described in Eq. 2. We use classical spin variables S_i^β , with $\beta = (x, y, z, 0)$. The initial states are sampled on the discrete phase space according to the distributions encoding the spin pointing down for all particles, i.e., we fix $S_i^z = -1$ and the spin components in the orthogonal direction are chosen randomly as $S_i^x, S_i^y = \pm 1$ with equal probability. In contrast to the closed DTWA [43], we also include classical variables S_i^0 , which encodes the local norm of a given site and is initialized to $S_i^0 = 1$. This additional degree of freedom is necessary because already the closed DTWA conserves the norm of the Bloch vector only after averaging over all trajectories, while our quantum-jump approach requires knowledge of the norm on the level of a single trajectory. Each spin of the state propagates under the effective non-Hermitian Hamiltonian $\hat{H}_i - i\gamma_d \hat{\sigma}_i^+ \hat{\sigma}_i^- / 2$. The corresponding semiclassical equations of motion are [47]

$$\dot{S}_i^x = -\frac{V}{2} S_i^y \sum_j S_j^z - \frac{\gamma_d}{2} S_i^x, \quad (4)$$

$$\dot{S}_i^y = \frac{V}{2} S_i^x \sum_j S_j^z - g S_i^z - \frac{\gamma_d}{2} S_i^y, \quad (5)$$

$$\dot{S}_i^z = g S_i^y - \frac{\gamma_d}{2} (S_i^z + S_i^0), \quad (6)$$

$$\dot{S}_i^0 = -\frac{\gamma_d}{2} (S_i^z + S_i^0), \quad (7)$$

with the sum over j being performed over the nearest neighbors of the spin i . Here, the interaction terms are incorporated on the level of a mean-field decoupling, as it is the case in the closed DTWA. Importantly, this mean-field decoupling is performed on the level of a single trajectory, therefore the ensemble average does not correspond to the mean-field equations of motion for the density operator. If desired, it is also possible to include higher orders of the Bogoliubov-Born-Green-Kirkwood-Yvon (BBGKY) hierarchy of correlation functions in the phase-point operators [55]. We numerically integrate the equations of motion using a fourth-order Runge Kutta

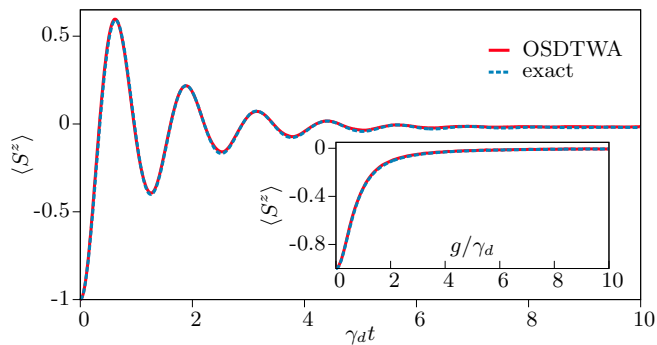


FIG. 2. Benchmarking against exact results for a single spin. The time evolution of $\langle S^z(t) \rangle$, same as in Fig. 1(b), is compared with the exact result $S_{\text{exact}}^z(t)$ for $g/\gamma_d = 5$. The inset shows the numerically obtained steady state from $\langle S^z(t) \rangle$ in the long-time limit and the exact steady state for varying g/γ_d .

method. The global norm $S^0(t) = \prod_i^N S_i^0(t)$ decreases under the time evolution from its initial value $S^0(0) = 1$. Once the global norm drops below a random number r drawn from a standard uniform distribution, a quantum jump occurs. Importantly, this approach allows to use a high-order numerical integrator for both the coherent and dissipative parts of the time evolution and thus yields a higher order of accuracy compared to direct approaches to solve the quantum master equation [58, 59]. The precise time τ of the quantum jump is determined by solving the equation $S^0(\tau) = r$.

Having determined the time of the quantum jump, we still need to choose which of the jump operators (i.e., on which site) is actually occurring. For this, we calculate the jump probability for spin i by $\delta p_i = (\prod_{j \neq i}^N S_j^0) \times \gamma_d (S_i^0 + S_i^z)/2$ [47]. The jump operator that is fired is then chosen to occur at site n such that n is the smallest integer satisfying $\sum_i^n P_i(\tau) \geq r$, where $P_i = \delta p_i / (\sum_i^N \delta p_i)$ is the normalized spin probability [59]. For the fired spin n , we set $S_n^z = -1$ and choose S_n^x and S_n^y randomly as ± 1 again with equal probability. For all other spins we normalize the spin fields by S_i^0 as $S_i^\beta = S_i^\beta / S_i^0$. We continue the time evolution by generating a different r and by repeating the above procedure, see Fig. 1(b). To avoid rare events leading to a divergence of the spin variables, we clip each individual spin variable to $|S_i^z| < \sqrt{3}$, which is the largest possible value that can be reached in an individual trajectory in a closed system. However, we find that this clipping is only necessary in the absence of interactions. In Fig. 1(b) we also show $\langle S^z(t) \rangle$, which initially displays oscillatory behavior and then eventually reaches a steady state.

Benchmarking the OSDTWA.— In the following, we compare the OSDTWA to the time evolution of a single spin, as in this case, the method does not introduce any additional errors from the mean-field decoupling in Eqs. (4–5) and the sampling of the phase space in terms

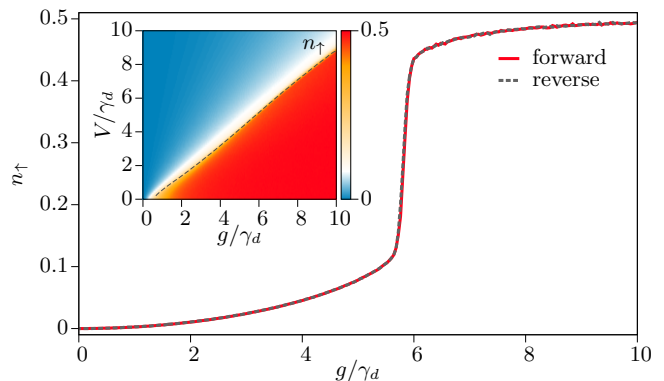


FIG. 3. Liquid-gas transition. The spin-up density n_\uparrow as a function of g/γ_d for $V/\gamma_d = 5$ for both the forward (continuous line) and reverse sweep (dashed line). The inset depicts n_\uparrow as a function of g/γ_d and V/γ_d , where the dashed line is the location of the susceptibility peak, see the main text. All results are shown for a 10×10 lattice and 3200 trajectories.

of a complete set of single-site operators is exact. We refer to this as the non-interacting case as it does not contain any spin-spin interactions. Hence, the OSDTWA should match the exact solution of the quantum master equation [60] in the limit of vanishing step size of the numerical integration. In Fig. 2 we compare the simulation result of $\langle S^z(t) \rangle$ with the exact result $S_{\text{exact}}^z(t)$ for $g/\gamma_d = 5$. Their comparison shows an excellent agreement; see also [47]. For the steady state $S_{\text{exact}}^z(t)$ yields the result $S_{\text{exact}}^z = -1/(1 + 2\tilde{g}^2)$, with $\tilde{g} = g/\gamma_d$. We therefore determine the numerical result of the steady state from $\langle S^z(t) \rangle$ in the long-time limit $t\gamma_d = 100$. In the inset of Fig. 2 we present the numerical and the exact result of the steady state as a function of g/γ_d . The steady state of the OSDTWA again agrees excellently with the exact steady state. Furthermore, we find the error in $\langle S_z \rangle$ scaling like $\Delta t^{6.15 \pm 0.22}$ with the integration step size Δt [47].

Another important consequence of our particular choice of the incorporation of quantum jumps is that the method becomes also exact when the dynamics is governed by classical rate equations. In this case, our approach yields a quantum-jump version of conventional kinetic Monte-Carlo methods [61].

Driven-dissipative criticality.— Let us now turn to the dissipative Ising model including the Ising interaction on a two-dimensional square lattice. From variational calculations [62], field-theoretical arguments [38], tensor network simulations [63], and cluster mean-field theory [64], it is known that the model exhibits a first-order transition for sufficiently strong interactions V , when varying the strength of the transverse field g . This transition can be understood as a liquid-gas transition of spin-up particles and the first-order transition line vanishes eventually in a critical point when decreasing V [41, 62]. Importantly, this transition is not due to spontaneous breaking

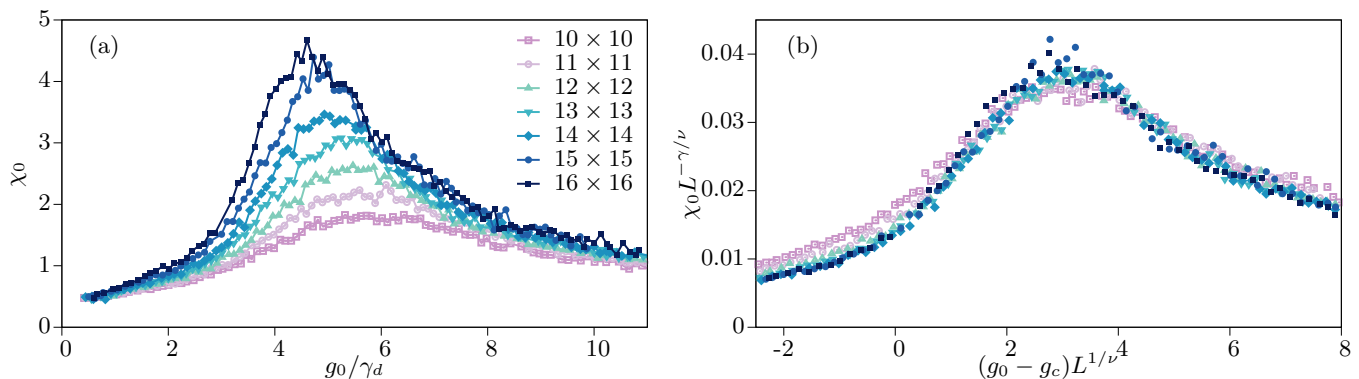


FIG. 4. Driven-dissipative criticality. (a) Value χ_0 and position g_0 of the susceptibility peak for varying system sizes between 10×10 and 16×16 , derived from Gaussian fits to the susceptibility $\chi(g) = (\partial n_\uparrow / \partial g)$. Results were obtained using up to 12,000 trajectories. (b) Universal scaling close to the critical point obtained by fitting the susceptibility data to the finite-size scaling function Eq. (8), which yields the critical exponents $\gamma = 1.69 \pm 0.07$ and $\nu = 0.99 \pm 0.04$, and the critical point $g_c/\gamma_d = 2.94 \pm 0.14$.

of the \mathbb{Z}_2 symmetry of the Hamiltonian (as this is already broken by the dissipation), but it is governed by the appearance of an emergent symmetry, similar to the liquid-gas transition in thermal equilibrium. Using mean-field analysis, the critical point has been predicted to belong to the Ising universality class [41], but it has not been possible to analyze the critical behavior going beyond a mean-field treatment.

To demonstrate that the OSDTWA is capable of capturing fluctuations beyond mean-field theory, we first consider a 10×10 lattice with periodic boundary conditions and $V/\gamma_d = 5$. We calculate the spin-up density $n_\uparrow = (1 + \langle S^z \rangle)/2$ using the steady state value of $\langle S^z(t) \rangle$ in a long-time limit. Starting from the solution at $g = 0$, we follow the steady state for g in the range $g/\gamma_d = [0, 10]$ using both a forward and a reverse sweep of g . In Fig. 3 we show the results of n_\uparrow as a function of g/γ_d for both cases of forward and reverse sweeps. The perfect overlap demonstrates that the steady state obtained within the OSDTWA is unique and not plagued by the mean-field artifact of bistability [20, 41]. In addition, the results of n_\uparrow manifest a first-order phase transition, since n_\uparrow undergoes a steep jump around $g/\gamma_d = 5.8$, which is also in very good quantitative agreement with previous numerical predictions [62]. In the inset of Fig. 3 we show n_\uparrow as a function of g/γ_d and V/γ_d . For intermediate and large V/γ_d , n_\uparrow indicates a sharp increase as g/γ_d is increased across the first-order transition. For small V , the change of n_\uparrow appears in a much broader region, suggesting that the first-order line eventually terminates in a critical point.

To investigate the critical behavior of the model, we determine the susceptibility $\chi(g) = (\partial n_\uparrow / \partial g)$ by taking a numerical derivative of n_\uparrow with respect to g . We fit $\chi(g)$ to the Gaussian function $f(g) = \chi_0 \exp(-(g - g_0)^2 / (2\sigma^2))$, with χ_0 , g_0 , and σ being the fitting parameters. g_0 gives the location of the susceptibility peak, which is indicated

as a dashed line in the inset of Fig. 3. χ_0 is the height of the susceptibility peak, which we use to determine the critical point below.

To identify the critical point and its properties, we calculate $\chi_0(g_0)$ for varying system sizes between 10×10 and 16×16 sites. All simulations employ periodic boundary conditions. In Fig. 4(a), we show $\chi_0(g_0)$ for the different system sizes, which displays a susceptibility peak diverging with system size. The precise nature of this divergence is controlled by the critical exponents of the transition, which in the framework of finite-size scaling theory [65] can be captured as

$$\chi_0(g_0, L) = L^{\gamma/\nu} f((g_0 - g_c)L^{1/\nu}), \quad (8)$$

where L is the linear dimension of the system, g_c is the critical point, and γ and ν are the critical exponents. Due to the hyperscaling relations [66], which can also be expected to hold for steady-state transitions obeying thermal statistics, two critical exponents are sufficient to fix all others as well. The analytic scaling function $f(x)$ is then expanded as a fourth-order polynomial and fitted to the results of χ_0 , which allows us to determine the critical parameters in the thermodynamic limit. From the fit, we obtain $g_c/\gamma_d = 2.94 \pm 0.14$, $\gamma = 1.69 \pm 0.07$, and $\nu = 0.99 \pm 0.04$. Using these results, we observe all susceptibility data to collapse on a single line, see Fig. 4(b), which demonstrates that we have correctly identified the critical exponents. Remarkably, the values of γ and ν are in very good agreement with $\gamma = 7/4$ and $\nu = 1$ of the 2D classical Ising model, i.e., the dissipative Ising model belongs to the same universality class. Furthermore, the OSDTWA value for the critical point $g_c/\gamma_d = 2.94 \pm 0.14$ lies between the predictions from the variational principle ($g_c/\gamma_d = 2.28$ [62]) and cluster mean-field theory ($g_c/\gamma_d = 4.88$ [64]).

Strikingly, the OSDTWA is able to capture fluctuations beyond mean-field theory, although the Ising in-

teraction is decoupled on a mean-field level. This can be attributed to the fact that classical fluctuations are correctly accounted for in our quantum-jump approach, while quantum fluctuations are irrelevant at the transition due to the presence of a dynamical symmetry yielding an effective field theory at finite temperature [37]. Interestingly, in this approach, the quantum fields are gapped and can be mapped onto classical fluctuation fields by means of a Hubbard-Stratonovich transformation [67], which is conceptually very similar to the random choices of the $S^{x,y}$ fields following a quantum jump within the OSDTWA.

Conclusions and outlook.— We have presented a novel simulation approach for an open quantum system based on the discrete truncated Wigner approximation. For the paradigmatic dissipative Ising model on a square lattice, we arrive at the first prediction of its critical behavior beyond mean-field theory, which we find to be consistent with the 2D Ising universality class. Importantly, our method can be expected to give reliable results for a large class of open quantum many-body systems governed by a dynamical symmetry. Additionally, despite its computational simplicity, our OSTDWA method can be used to obtain novel insights into non-critical many-body problems that are notoriously hard to simulate, such as strongly interacting Rydberg polaritons [68–70]. Finally, in future studies it will be interesting to see whether the OSTDWA can also capture open many-body systems displaying non-thermal critical behavior, as it has been recently reported for quantum versions of absorbing state models [71].

Note added: During preparation of our manuscript, we became aware of a related work employing a quantum state diffusion approach to the discrete TWA [72].

Acknowledgments.— This work was funded by the Volkswagen Foundation, by the Deutsche Forschungsgemeinschaft (DFG, German Research Foundation) within Project-ID 274200144 – SFB 1227 (DQ-mat, Project No. A04), SPP 1929 (GiRyd), and under Germany’s Excellence Strategy–EXC-2123 QuantumFrontiers–390837967.

-
- [1] S. Diehl, A. Micheli, A. Kantian, B. Kraus, H. P. Büchler, and P. Zoller, Quantum states and phases in driven open quantum systems with cold atoms, *Nature Physics* **4**, 878 (2008).
- [2] F. Verstraete, M. M. Wolf, and J. Ignacio Cirac, Quantum computation and quantum-state engineering driven by dissipation, *Nature Phys.* **5**, 633 (2009).
- [3] H. Weimer, M. Müller, I. Lesanovsky, P. Zoller, and H. P. Büchler, A Rydberg quantum simulator, *Nature Phys.* **6**, 382 (2010).
- [4] H. Krauter, C. A. Muschik, K. Jensen, W. Wasilewski, J. M. Petersen, J. I. Cirac, and E. S. Polzik, Entanglement Generated by Dissipation and Steady State Entanglement of Two Macroscopic Objects, *Phys. Rev. Lett.* **107**, 080503 (2011).
- [5] J. T. Barreiro, M. Müller, P. Schindler, D. Nigg, T. Monz, M. Chwalla, M. Hennrich, C. F. Roos, P. Zoller, and R. Blatt, An open-system quantum simulator with trapped ions, *Nature* **470**, 486 (2011).
- [6] A. W. Carr and M. Saffman, Preparation of Entangled and Antiferromagnetic States by Dissipative Rydberg Pumping, *Phys. Rev. Lett.* **111**, 033607 (2013).
- [7] D. D. B. Rao and K. Mølmer, Dark Entangled Steady States of Interacting Rydberg Atoms, *Phys. Rev. Lett.* **111**, 033606 (2013).
- [8] G. Morigi, J. Eschner, C. Cormick, Y. Lin, D. Leibfried, and D. J. Wineland, Dissipative Quantum Control of a Spin Chain, *Phys. Rev. Lett.* **115**, 200502 (2015).
- [9] F. Reiter, D. Reeb, and A. S. Sørensen, Scalable Dissipative Preparation of Many-Body Entanglement, *Phys. Rev. Lett.* **117**, 040501 (2016).
- [10] M. Roghani and H. Weimer, Dissipative preparation of entangled many-body states with Rydberg atoms, *Quantum Sci. Technol.* **3**, 035002 (2018).
- [11] M. Raghunandan, F. Wolf, C. Ospelkaus, P. O. Schmidt, and H. Weimer, Initialization of quantum simulators by sympathetic cooling, *Science Advances* **6**, eaaw9268 (2020).
- [12] M. Metcalf, J. E. Moussa, W. A. de Jong, and M. Sarovar, Engineered thermalization and cooling of quantum many-body systems, *Phys. Rev. Research* **2**, 023214 (2020).
- [13] J. Kasprzak, M. Richard, S. Kundermann, A. Baas, P. Jeambrun, J. M. J. Keeling, F. M. Marchetti, M. H. Szymańska, R. André, J. L. Staehli, V. Savona, P. B. Littlewood, B. Deveaud, and L. S. Dang, Bose–Einstein condensation of exciton polaritons, *Nature* **443**, 409 (2006).
- [14] A. Amo, D. Sanvitto, F. P. Laussy, D. Ballarini, E. d. Valle, M. D. Martin, A. Lemaître, J. Bloch, D. N. Krizhanovskii, M. S. Skolnick, C. Tejedor, and L. Viña, Collective fluid dynamics of a polariton condensate in a semiconductor microcavity, *Nature* **457**, 291 (2009).
- [15] M. J. Hartmann, Polariton Crystallization in Driven Arrays of Lossy Nonlinear Resonators, *Phys. Rev. Lett.* **104**, 113601 (2010).
- [16] K. Baumann, C. Guerlin, F. Brennecke, and T. Esslinger, Dicke quantum phase transition with a superfluid gas in an optical cavity, *Nature* **464**, 1301 (2010).
- [17] D. Nagy, G. Kónya, G. Szirmai, and P. Domokos, Dicke-Model Phase Transition in the Quantum Motion of a Bose-Einstein Condensate in an Optical Cavity, *Phys. Rev. Lett.* **104**, 130401 (2010).
- [18] S. Diehl, A. Tomadin, A. Micheli, R. Fazio, and P. Zoller, Dynamical Phase Transitions and Instabilities in Open Atomic Many-Body Systems, *Phys. Rev. Lett.* **105**, 015702 (2010).
- [19] A. Tomadin, S. Diehl, and P. Zoller, Nonequilibrium phase diagram of a driven and dissipative many-body system, *Phys. Rev. A* **83**, 013611 (2011).
- [20] T. E. Lee, H. Häffner, and M. C. Cross, Antiferromagnetic phase transition in a nonequilibrium lattice of Rydberg atoms, *Phys. Rev. A* **84**, 031402(R) (2011).
- [21] E. M. Kessler, G. Giedke, A. Imamoglu, S. F. Yelin, M. D. Lukin, and J. I. Cirac, Dissipative phase transition in a central spin system, *Phys. Rev. A* **86**, 012116 (2012).
- [22] M. Höning, M. Moos, and M. Fleischhauer, Critical exponents of steady-state phase transitions in fermionic lattice models, *Phys. Rev. A* **86**, 013606 (2012).

- [23] M. Höning, D. Muth, D. Petrosyan, and M. Fleischhauer, Steady-state crystallization of Rydberg excitations in an optically driven lattice gas, *Phys. Rev. A* **87**, 023401 (2013).
- [24] A. Le Boité, G. Orso, and C. Ciuti, Steady-State Phases and Tunneling-Induced Instabilities in the Driven Dissipative Bose-Hubbard Model, *Phys. Rev. Lett.* **110**, 233601 (2013).
- [25] B. Horstmann, J. I. Cirac, and G. Giedke, Noise-driven dynamics and phase transitions in fermionic systems, *Phys. Rev. A* **87**, 012108 (2013).
- [26] E. G. D. Torre, S. Diehl, M. D. Lukin, S. Sachdev, and P. Strack, Keldysh approach for nonequilibrium phase transitions in quantum optics: Beyond the Dicke model in optical cavities, *Phys. Rev. A* **87**, 023831 (2013).
- [27] J. Qian, L. Zhou, and W. Zhang, Quantum phases of strongly interacting Rydberg atoms in triangular lattices, *Phys. Rev. A* **87**, 063421 (2013).
- [28] T. E. Lee, S. Gopalakrishnan, and M. D. Lukin, Unconventional Magnetism via Optical Pumping of Interacting Spin Systems, *Phys. Rev. Lett.* **110**, 257204 (2013).
- [29] C. Joshi, F. Nissen, and J. Keeling, Quantum correlations in the one-dimensional driven dissipative XY model, *Phys. Rev. A* **88**, 063835 (2013).
- [30] N. Lang and H. P. Büchler, Exploring quantum phases by driven dissipation, *Phys. Rev. A* **92**, 012128 (2015).
- [31] J. Marino and S. Diehl, Driven Markovian Quantum Criticality, *Phys. Rev. Lett.* **116**, 070407 (2016).
- [32] M. Marcuzzi, M. Buchhold, S. Diehl, and I. Lesanovsky, Absorbing State Phase Transition with Competing Quantum and Classical Fluctuations, *Phys. Rev. Lett.* **116**, 245701 (2016).
- [33] H. Weimer, Tailored jump operators for purely dissipative quantum magnetism, *J. Phys. B* **50**, 024001 (2017).
- [34] C. D. Parmee and N. R. Cooper, Phases of driven two-level systems with nonlocal dissipation, *Phys. Rev. A* **97**, 053616 (2018).
- [35] E. T. Owen, J. Jin, D. Rossini, R. Fazio, and M. J. Hartmann, Quantum correlations and limit cycles in the driven-dissipative Heisenberg lattice, *New Journal of Physics* **20**, 045004 (2018).
- [36] A. Jamadagni and H. Weimer, An Operational Definition of Topological Order, [arXiv:2005.06501](https://arxiv.org/abs/2005.06501) (2020).
- [37] L. M. Sieberer, S. D. Huber, E. Altman, and S. Diehl, Dynamical Critical Phenomena in Driven-Dissipative Systems, *Phys. Rev. Lett.* **110**, 195301 (2013).
- [38] M. F. Maghrebi and A. V. Gorshkov, Nonequilibrium many-body steady states via Keldysh formalism, *Phys. Rev. B* **93**, 014307 (2016).
- [39] C. Carr, R. Ritter, C. G. Wade, C. S. Adams, and K. J. Weatherill, Nonequilibrium Phase Transition in a Dilute Rydberg Ensemble, *Phys. Rev. Lett.* **111**, 113901 (2013).
- [40] N. Malossi, M. M. Valado, S. Scotto, P. Huillery, P. Pillet, D. Ciampini, E. Arimondo, and O. Morsch, Full Counting Statistics and Phase Diagram of a Dissipative Rydberg Gas, *Phys. Rev. Lett.* **113**, 023006 (2014).
- [41] M. Marcuzzi, E. Levi, S. Diehl, J. P. Garrahan, and I. Lesanovsky, Universal Nonequilibrium Properties of Dissipative Rydberg Gases, *Phys. Rev. Lett.* **113**, 210401 (2014).
- [42] H. Weimer, A. Kshetrimayum, and R. Orús, Simulation methods for open quantum many-body systems, *Rev. Mod. Phys.* **93**, 015008 (2021).
- [43] J. Schachenmayer, A. Pikovski, and A. M. Rey, Many-Body Quantum Spin Dynamics with Monte Carlo Trajectories on a Discrete Phase Space, *Phys. Rev. X* **5**, 011022 (2015).
- [44] J. Dalibard, Y. Castin, and K. Mølmer, Wave-function approach to dissipative processes in quantum optics, *Phys. Rev. Lett.* **68**, 580 (1992).
- [45] R. Dum, P. Zoller, and H. Ritsch, Monte Carlo simulation of the atomic master equation for spontaneous emission, *Phys. Rev. A* **45**, 4879 (1992).
- [46] K. Mølmer, Y. Castin, and J. Dalibard, Monte Carlo wave-function method in quantum optics, *J. Opt. Soc. Am. B* **10**, 524 (1993).
- [47] See Supplemental Material for the derivation of the equations of motion and the jump probability, the comparison with exact results, and the OSDTWA analysis of the dissipative XYZ model.
- [48] I. Carusotto and C. Ciuti, Spontaneous microcavity-polariton coherence across the parametric threshold: Quantum Monte Carlo studies, *Phys. Rev. B* **72**, 125335 (2005).
- [49] I. Carusotto and C. Ciuti, Quantum fluids of light, *Rev. Mod. Phys.* **85**, 299 (2013).
- [50] G. Dagvadorj, J. M. Fellows, S. Matyjaśkiewicz, F. M. Marchetti, I. Carusotto, and M. H. Szymańska, Nonequilibrium Phase Transition in a Two-Dimensional Driven Open Quantum System, *Phys. Rev. X* **5**, 041028 (2015).
- [51] F. Vicentini, F. Minganti, R. Rota, G. Orso, and C. Ciuti, Critical slowing down in driven-dissipative Bose-Hubbard lattices, *Phys. Rev. A* **97**, 013853 (2018).
- [52] J. Huber, P. Kirton, and P. Rabl, Phase-Space Methods for Simulating the Dissipative Many-Body Dynamics of Collective Spin Systems, *SciPost Phys.* **10**, 45 (2021).
- [53] A. Polkovnikov, Phase space representation of quantum dynamics, *Annals of Physics* **325**, 1790 (2010).
- [54] W. K. Wootters, A Wigner-function formulation of finite-state quantum mechanics, *Annals of Physics* **176**, 1 (1987).
- [55] S. Czischek, M. Gärttner, M. Oberthaler, M. Kastner, and T. Gasenzer, Quenches near criticality of the quantum Ising chain—power and limitations of the discrete truncated Wigner approximation, *Quantum Science and Technology* **4**, 014006 (2018).
- [56] S. Sachdev, *Quantum Phase Transitions* (Cambridge University Press, Cambridge, 1999).
- [57] H. Weimer, Variational analysis of driven-dissipative Rydberg gases, *Phys. Rev. A* **91**, 063401 (2015).
- [58] A. J. Daley, Quantum trajectories and open many-body quantum systems, *Adv. Phys.* **63**, 77 (2014).
- [59] J. Johansson, P. Nation, and F. Nori, QuTiP: An open-source Python framework for the dynamics of open quantum systems, *Comp. Phys. Comm.* **183**, 1760 (2012).
- [60] H.-P. Breuer and F. Petruccione, *The Theory of Open Quantum Systems* (Oxford University Press, Oxford, 2002).
- [61] A. Bortz, M. Kalos, and J. Lebowitz, A new algorithm for Monte Carlo simulation of Ising spin systems, *J. Comp. Phys.* **17**, 10 (1975).
- [62] H. Weimer, Variational Principle for Steady States of Dissipative Quantum Many-Body Systems, *Phys. Rev. Lett.* **114**, 040402 (2015).
- [63] A. Kshetrimayum, H. Weimer, and R. Orús, A simple tensor network algorithm for two-dimensional steady states, *Nature Commun.* **8**, 1291 (2017).
- [64] J. Jin, A. Biella, O. Viyuela, C. Ciuti, R. Fazio, and

- D. Rossini, Phase diagram of the dissipative quantum Ising model on a square lattice, *Phys. Rev. B* **98**, 241108(R) (2018).
- [65] J. L. Cardy, *Scaling and Renormalization in Statistical Physics* (Cambridge University Press, Cambridge, 1996).
- [66] K. Huang, *Statistical Mechanics* (John Wiley and Sons, New York, 1987).
- [67] L. M. Sieberer, M. Buchhold, and S. Diehl, Keldysh field theory for driven open quantum systems, *Rep. Prog. Phys.* **79**, 096001 (2016).
- [68] A. V. Gorshkov, J. Otterbach, M. Fleischhauer, T. Pohl, and M. D. Lukin, Photon-Photon Interactions via Rydberg Blockade, *Phys. Rev. Lett.* **107**, 133602 (2011).
- [69] T. Peyronel, O. Firstenberg, Q.-Y. Liang, S. Hofferberth, A. V. Gorshkov, T. Pohl, M. D. Lukin, and V. Vuletić, Quantum nonlinear optics with single photons enabled by strongly interacting atoms, *Nature* **488**, 57 (2012).
- [70] T. Pistorius, J. Kazemi, and H. Weimer, Quantum Many-Body Dynamics of Driven-Dissipative Rydberg Polaritons, *Phys. Rev. Lett.* **125**, 263604 (2020).
- [71] F. Carollo, E. Gillman, H. Weimer, and I. Lesanovsky, Critical Behavior of the Quantum Contact Process in One Dimension, *Phys. Rev. Lett.* **123**, 100604 (2019).
- [72] J. Huber, A. M. Rey, and P. Rabl, Realistic simulations of spin squeezing and cooperative coupling effects in large ensembles of interacting two-level systems, *Phys. Rev. A* **105**, 013716 (2022).

Supplemental Material for “Driven-dissipative criticality within the discrete truncated Wigner approximation”

Vijay Pal Singh^{1,2} and Hendrik Weimer¹

¹*Institut für Theoretische Physik, Leibniz Universität Hannover, Appelstraße 2, 30167 Hannover, Germany*

²*Zentrum für Optische Quantentechnologien and Institut für Laserphysik, Universität Hamburg, 22761 Hamburg, Germany*

MONTE-CARLO WAVE-FUNCTION FORMALISM

We describe the open-system dynamics using the quantum master equation in Lindblad form

$$\frac{d}{dt}\rho = -i[H, \rho] + \sum_i \left(c_i \rho c_i^\dagger - \frac{1}{2} \{c_i^\dagger c_i, \rho\} \right), \quad (\text{S1})$$

where ρ is the density matrix describing the ensemble average of a quantum system, H is the system Hamiltonian, and c_i are the collapse operators. We rewrite Eq. (S1) as

$$\dot{\rho} = -i(H_{\text{eff}}\rho - \rho H_{\text{eff}}^\dagger) + \sum_i c_i \rho c_i^\dagger, \quad (\text{S2})$$

where

$$H_{\text{eff}} = H - \frac{i}{2} \sum_i c_i^\dagger c_i \quad (\text{S3})$$

is the non-Hermitian effective Hamiltonian for the dissipative system. The term $\sum_i c_i \rho c_i^\dagger$ in Eq. S2 is referred to as the recycling term [1]. For a two-level system with decay from an excited state to the ground state, the non-Hermitian part can be thought of as removing amplitude from the excited state and the recycling term as restoring it in the ground state.

Following Refs. [2, 3], the time evolution of $\rho(t)$ can be described in terms of quantum jumps and nonunitary evolution between these jumps via [4]

$$\rho(t) = \sum_{n=0}^{\infty} \sum_{\gamma_1, \dots, \gamma_n} \int_{t_0}^t dt_n \int_{t_0}^{t_n} dt_{n-1} \dots \int_{t_0}^{t_2} dt_1 S_{tt_n} c_{\gamma_n} S_{t_n t_{n-1}} \dots S_{t_2 t_1} c_{\gamma_1} S_{t_1 t_0} \rho(t_0), \quad (\text{S4})$$

with

$$S_{tt_0} \rho(t_0) = e^{-iH_{\text{eff}}(t-t_0)} \rho(t_0) e^{iH_{\text{eff}}^\dagger(t-t_0)}. \quad (\text{S5})$$

The indices $n = 0, 1, 2, \dots$ and $\gamma_1, \dots, \gamma_n$ account for contributions to the density matrix from the subensemble that has undergone exactly n quantum jumps at times $t > t_n \geq \dots \geq t_1 \geq t_0$ with a sequence of realizations $\gamma_1, \dots, \gamma_n$. To construct a wave-function representation we use $\rho(t_0) = \sum_{\alpha} p_{\alpha} |\alpha\rangle\langle\alpha|$ ($0 \leq p_{\alpha} \leq 1$ and $\sum_{\alpha} p_{\alpha} = 1$) and obtain

$$\rho(t) = \sum_{\alpha} \sum_{n=0}^{\infty} \sum_{\gamma_1, \dots, \gamma_n} \int_{t_0}^t dt_n \int_{t_0}^{t_n} dt_{n-1} \dots \int_{t_0}^{t_2} dt_1 |\phi(t|t_n, \gamma_n; \dots; t_1, \gamma_1; \alpha)\rangle \langle\phi(t|t_n, \gamma_n; \dots; t_1, \gamma_1; \alpha)| p_{\alpha}, \quad (\text{S6})$$

where $|\phi(t|t_n, \gamma_n; \dots; \alpha)\rangle$ are a hierarchy of system wave functions that follow

$$i \frac{d}{dt} |\phi(t|t_n, \gamma_n; \dots)\rangle = H_{\text{eff}} |\phi(t|t_n, \gamma_n; \dots)\rangle \quad (\text{S7})$$

for $t \geq t_n$ with initial condition $|\phi(t_0|\alpha)\rangle = |\alpha\rangle$.

Eq. (S6) enables a wave function simulation of the density matrix in terms of Monte Carlo wave functions (MCWFs). The initial state is sampled from the density matrix $\rho(t=0)$ at time $t=0$. The simulation procedure is as follows.

1. We start with a normalized wave function $|\psi(0)\rangle$.

2. We choose a random number r between 0 and 1, which corresponds to the probability that a quantum jump occurs.
3. We numerically propagate $|\psi(t)\rangle$ according to H_{eff} , i.e.,

$$i \frac{d}{dt} |\psi(t)\rangle = H_{\text{eff}} |\psi(t)\rangle \quad (\text{S8})$$

and determine the quantum jump time t by solving $\langle \psi(t) | \psi(t) \rangle = r$, where $\langle \psi(t) | \psi(t) \rangle$ is the norm.

4. At time t , the resulting jump operator projects the system into one of the renormalized states given by

$$|\psi(t^+)\rangle = \frac{c_i |\psi(t^-)\rangle}{\langle \psi(t^-) | c_i^\dagger c_i | \psi(t^-) \rangle^{1/2}}, \quad (\text{S9})$$

where $|\psi(t^-)\rangle$ is the wave function propagating in time up to time t and $|\psi(t^+)\rangle$ is the state after the jump. The corresponding jump operator is chosen such that l is the smallest integer satisfying $\sum_{i=1}^l P_i(t) \geq r$, where $P_i = \delta p_i / \sum_i \delta p_i$ is the normalized probability, with

$$\delta p_i = \langle \psi(t) | c_i^\dagger c_i | \psi(t) \rangle. \quad (\text{S10})$$

5. We now continue the time evolution with the renormalized state from step 4 and draw a new random number r . This process is repeated until the final simulation time is reached.

The MCWF approach determines the time evolution on the level of a single trajectory. By repeating the time evolution over different initial wave functions, an ensemble of the trajectories is obtained, giving the time evolution that is equivalent to the quantum master equation in Eq. (S1), i.e.,

$$\rho(t) = \left\langle \left\langle \frac{|\psi(t)\rangle \langle \psi(t)|}{\langle \psi(t) | \psi(t) \rangle} \right\rangle \right\rangle, \quad (\text{S11})$$

where $\langle \langle \ \rangle \rangle$ denotes an average over many trajectories.

OPEN-SYSTEM DISCRETE TRUNCATED WIGNER APPROXIMATION (OSDTWA)

Derivation of equations of motion

To obtain a semiclassical description of open quantum systems, we establish an open-system variant of the discrete truncated Wigner approximation. This includes a semiclassical approximation of the density matrix, i.e., we sample the initial state from the discrete truncated Wigner approximation (DTWA). Furthermore, the time evolution is obtained on the level of individual trajectories within the quantum-jump formalism, which is discussed in the previous section. As an application of our method, we consider the dissipative Ising model on a square lattice. The transverse-field Ising Hamiltonian is

$$H = \frac{g}{2} \sum_i \sigma_i^x + \frac{V}{4} \sum_{\langle ij \rangle} \sigma_i^z \sigma_j^z, \quad (\text{S12})$$

where g is the transverse field and V is the nearest neighbor interaction. σ_i^α are the Pauli operators at site i , with $\alpha = (x, y, z)$. The dissipative terms in Eq. (S1) occur in terms of spin-flip operators $c_i = \sqrt{\gamma_d} \sigma_i^-$, with γ_d being the decay rate of the up spins and $\sigma_i^\pm = (\sigma_i^x \pm i\sigma_i^y)/2$. Eq. (S1) results in

$$\dot{\rho} = -i(H_i \rho - \rho H_i) - \frac{\gamma_d}{2} \sigma_i^+ \sigma_i^- \rho - \frac{\gamma_d}{2} \rho \sigma_i^+ \sigma_i^- + \gamma_d \sigma_i^- \rho \sigma_i^+ \quad (\text{S13})$$

$$= -i(H_{\text{eff},i} \rho - \rho H_{\text{eff},i}^\dagger) + \gamma_d \sigma_i^- \rho \sigma_i^+, \quad (\text{S14})$$

where

$$H_{\text{eff},i} = H_i - i \frac{\gamma_d}{2} \sigma_i^+ \sigma_i^-. \quad (\text{S15})$$

In the quantum-jump approach the system propagates under H_{eff} between two quantum jumps, hence the phase-space variables also evolve under H_{eff} within the OSDTWA. The generalized phase-point operator is given by

$$\wp_i(\mathbf{r}_i) = (\sigma_i^0 + \mathbf{r}_i \cdot \boldsymbol{\sigma}_i)/2, \quad (\text{S16})$$

where $\boldsymbol{\sigma}_i = (\sigma_i^x, \sigma_i^y, \sigma_i^z)$ is the Pauli vector, and σ_i^0 is included to allow sampling from unnormalized density matrices. In our semiclassical approximation we use classical spin variables S_i^β , with $\beta = (x, y, z, 0)$. With the parametrization $\mathbf{r}_i(t) = (S_i^x, S_i^y, S_i^z)$, Eq. (S16) results in

$$\tilde{\wp}_i(\mathbf{r}_i) = \frac{1}{2}(S_i^0 \cdot \mathbf{1}_i + \mathbf{r}_i \cdot \boldsymbol{\sigma}_i) = \begin{pmatrix} \frac{1}{2}(S_i^0 + S_i^z) & S_i^- \\ S_i^+ & \frac{1}{2}(S_i^0 - S_i^z) \end{pmatrix}. \quad (\text{S17})$$

S_i^0 represents the norm of the spin state, i.e., $S_i^0 = \text{Tr}[\tilde{\wp}_i]$. The time evolution of $\tilde{\wp}_i(t)$ under H_{eff} as described in Eq. S14 is given by

$$\begin{pmatrix} \frac{1}{2}(\dot{S}_i^0 + \dot{S}_i^z) & \dot{S}_i^- \\ \dot{S}_i^+ & \frac{1}{2}(\dot{S}_i^0 - \dot{S}_i^z) \end{pmatrix} = \frac{1}{2} \begin{pmatrix} gS_i^y - \gamma_d(S_i^0 + S_i^z) & igS_i^z - S_i^-(\gamma_d + 4iV_j) \\ -igS_i^z - S_i^+(\gamma_d - 4iV_j) & -gS_i^y \end{pmatrix}, \quad (\text{S18})$$

which results in

$$\dot{S}_i^x = -2V_j S_i^y - \frac{\gamma_d}{2} S_i^x, \quad (\text{S19})$$

$$\dot{S}_i^y = 2V_j S_i^x - gS_i^z - \frac{\gamma_d}{2} S_i^y, \quad (\text{S20})$$

$$\dot{S}_i^z = gS_i^y - \frac{\gamma_d}{2}(S_i^z + S_i^0), \quad (\text{S21})$$

$$\dot{S}_i^0 = -\frac{\gamma_d}{2}(S_i^z + S_i^0), \quad (\text{S22})$$

where $V_j \equiv (V/4) \sum_j S_j^z$ and the index j runs over the nearest neighbors of site i .

The quantum jump probability, as described in Eq. (S10), is determined from the decay of the state, which is

$$\delta p_i = \text{Tr}[\tilde{\wp}_i c_i^\dagger c_i] = \gamma_d \text{Tr}[\tilde{\wp}_i \sigma_i^+ \sigma_i^-] = \frac{\gamma_d}{2}(S_i^0 + S_i^z). \quad (\text{S23})$$

For more than a single site, we calculate the jump probability at site i via

$$\delta p_i = \frac{\gamma_d}{2}(S_i^0 + S_i^z) \times \prod_{k \neq i}^N S_k^0, \quad (\text{S24})$$

where $\prod_{k \neq i}^N S_k^0$ is a normalization factor coming from all other sites than the site $i = k$.

Implementation of the OSDTWA

As we describe in the main text, we sample the initial state from the discrete truncated Wigner approximation. This is done by fixing $S_i^z = -1$ and randomly choosing $S_i^x, S_i^y = \pm 1$ with equal probability. S_i^0 represents the local norm of a given site and is initialized to $S_i^0 = 1$. Using a fourth-order Runge Kutta method, we numerically integrate the equations of motion in Eqs. (S19–S22). Once the global norm $S^0(t) = \prod_{i=1}^N S_i^0(t)$ drops below a random number r drawn from a standard uniform distribution, a quantum jump occurs. The precise quantum jump time τ is determined by solving the equation $S^0(\tau) = r$ using the Ridders' method. To choose the jump operator, we calculate the jump probability for spin i using Eq. (S24). The jump operator that is fired is then chosen to occur at site n such that n is the smallest integer satisfying $\sum_{i=1}^n P_i(\tau) \geq r$, where $P_i = \delta p_i / (\sum_i \delta p_i)$ is the normalized spin probability. For the fired spin n , we set $S_n^z = -1$ and choose S_n^x and S_n^y randomly as ± 1 again with equal probability. For all other spins we normalize the spin fields by S_i^0 as $S_i^\beta = S_i^\beta / S_i^0$. Afterwards, we continue the time evolution by generating a different r and by repeating the above procedure. Note that these steps are equivalent to the MCWF formalism discussed in the previous section. With the above procedure, we obtain the time evolution of a single trajectory, which undergoes several quantum jumps and nonunitary evolution between these jumps. By generating different initial configurations and different times of the quantum jumps, we obtain an ensemble of the trajectories. As the key observable, we calculate the averaged spin value in the z direction, i.e., $\langle S^z \rangle = (1/n_t) \sum_i^{n_t} S_i^z$, where n_t is the number of trajectories.

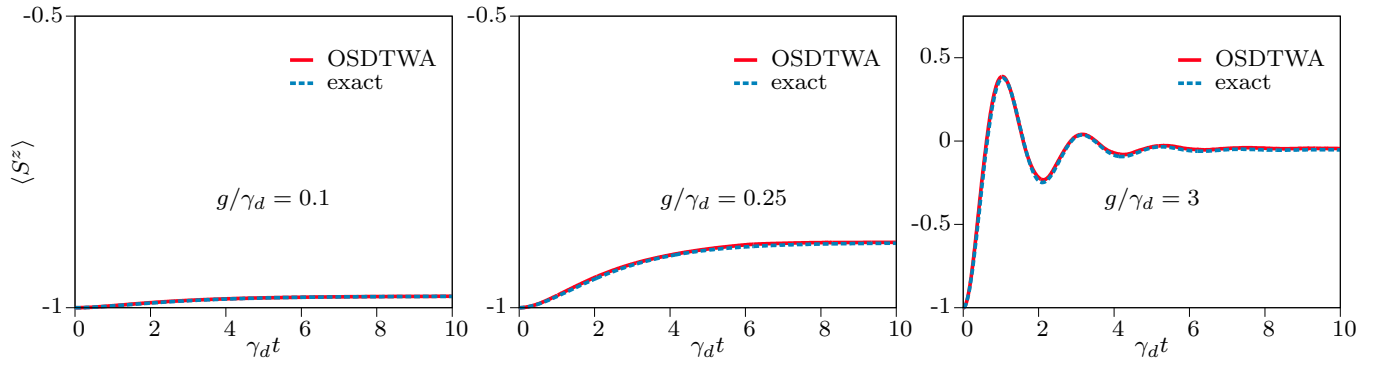


FIG. S1. Comparison with exact results. The time evolution of $\langle S^z(t) \rangle$, averaged over 10^5 trajectories, is compared with the exact result $S_{\text{exact}}^z(t)$ for $g/\gamma_d = 0.1, 0.25$, and 3.

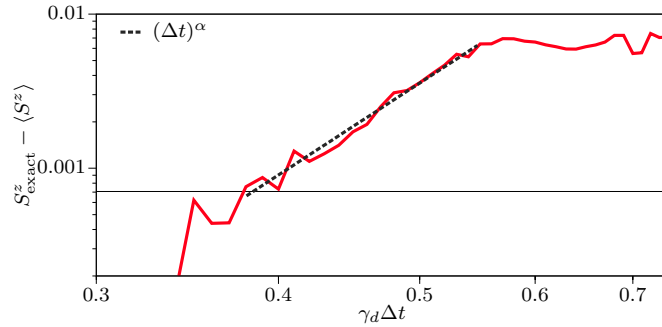


FIG. S2. The residual of $S_{\text{exact}}^z(t_0) - \langle S^z(t_0) \rangle$ for step size Δt and fixed $t_0\gamma_d = 50$, where the simulation result is averaged over 2 million trajectories and $g/\gamma_d = 5$. The dashed line is the fit proportional to $\Delta t^{6.15 \pm 0.22}$. The horizontal line indicates the noise floor from the total number of trajectories.

To confirm that the OSDTWA is exact in the noninteracting limit, we compare the OSDTWA to the time evolution of a single spin, as in this case, the method does not include any additional errors from the interaction terms in Eqs. (S19) and (S20). Hence, the OSDTWA should match the exact solution of the quantum master equation in the limit of vanishing step size of the numerical integration. For the exact result, we have [5]

$$S_{\text{exact}}^z(t) = \frac{2\tilde{g}^2}{1 + 2\tilde{g}^2} \left(1 - \exp(-3\tilde{t}/4) \left(\cos(\sqrt{\tilde{g}^2 - 1/16}\tilde{t}) + \frac{3 \sin(\sqrt{\tilde{g}^2 - 1/16}\tilde{t})}{\sqrt{\tilde{g}^2 - 1/16}} \right) \right) - 1, \quad (\text{S25})$$

with $\tilde{g} = g/\gamma_d$ and $\tilde{t} = t\gamma_d$. In Fig. S1 we compare the time evolution of $\langle S^z(t) \rangle$ with the exact result $S_{\text{exact}}^z(t)$ for $g/\gamma_d = 0.1, 0.25$, and 3. The OSDTWA and the exact result show excellent agreement. The weakly-damped limit occurs when $S_{\text{exact}}^z(t)$ yields an oscillatory motion in time, which is visible for $g/\gamma_d = 3$ in Fig. S1. The oscillatory behavior vanishes when \tilde{g} approaches the critical value $\tilde{g}_{\text{critical}} = 0.25$ and Eq. (S25) becomes $S_{\text{exact}}^z(t) = [1 - \exp(-3\tilde{t}/4) \times (1 + 3\tilde{t}/4)]/9 - 1$. We show this exact result and the OSDTWA for $g/\gamma_d = 0.25$ in Fig. S1. For \tilde{g} lower than $\tilde{g}_{\text{critical}}$, the system is overdamped, as we show the result at $g/\gamma_d = 0.1$ in Fig. S1.

For any numerical integration method, it is crucial to determine the scaling of the error with the size of the integration step Δt . To investigate this behavior, we examine the difference to the exact solution in the steady state as a function of Δt . As shown in Fig. S2, we observe a power-law scaling of the error proportional to $\Delta t^{6.15 \pm 0.22}$, which is even better than the Δt^5 scaling of the Runge-Kutta method for a single integration step. This improvement can be attributed to the robustness of the steady state to step size errors [6], which is a generic feature of open quantum systems.

Offdiagonal coherence at the transition

One important question concerning phase transitions in open quantum many-body systems is their degree of quantumness, especially since they inherently involve mixed quantum states. To address this question, we analyze the

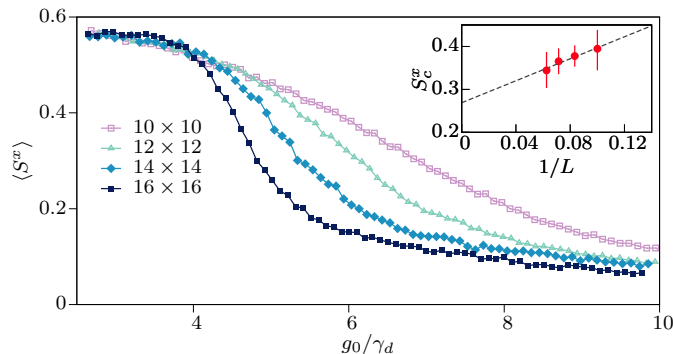


FIG. S3. Steady state value of $\langle S^x \rangle$ as a function of g_0 for varying system sizes between 10×10 and 16×16 , where g_0 represents the location of line of the liquid-gas transition. Results are obtained using trajectory numbers between 640 and 1920. We determine the values of $\langle S^x \rangle$ at the critical point $g_c(L)$ and show them as a function of $1/L$ in the inset plot, with L being the linear dimension of the system. The error bar is due to the uncertainty in the location of $g_c(L)$; see text. Using a linear fit (continuous line), we determine the critical value $S_c^x = 0.27 \pm 0.01$ in the thermodynamic limit.

steady-state value of the $\langle S^x \rangle$ observable, which is an offdiagonal coherence with respect to the $\langle S^z \rangle$ observable capturing the liquid-gas transition of the dissipative Ising model. We focus on $\langle S^x \rangle$ at the location g_0 of the susceptibility peak (i.e., along the curve of the liquid-gas transition), whose value and location are used to characterize the transition in the main text. In Fig. S3 we show $\langle S^x \rangle$ as a function of g_0 for various system sizes between 10×10 and 16×16 . For g_0 below $g_0/\gamma_d < 4$, the value of $\langle S^x \rangle$ is large and depends very weakly on the system size. In the intermediate regime of g_0/γ_d between 4 and 8, $\langle S^x \rangle$ undergoes a noticeable change depending on the system size. This suggests that off-diagonal coherences are important to describe the critical behavior. We determine the location $g_c(L)$ of the critical point from the susceptibility curves shown in the main text, where L is the linear dimension of the system. We calculate $\langle S^x \rangle$ at $g_c(L)$, finding a $1/L$ decay with system size, see the inset of Fig. S3. From this, we can determine the critical value in the thermodynamic limit as $S_c^x(L \rightarrow \infty) = 0.27 \pm 0.01$. This shows that offdiagonal coherence is persisting at criticality.

CRITICAL BEHAVIOR OF THE DISSIPATIVE XYZ MODEL

In the following, we use the OSDTWA to examine the criticality of the dissipative XYZ model on a square lattice, which exhibits a phase transition of the steady state between a paramagnetic and a ferromagnetic phase, as first suggested by mean-field predictions of Ref. [7]. This dissipative model has been analyzed using tensor network [8, 9] and cluster mean-field [10] methods. Using a tree tensor network approach, it was suggested that the phase transition belongs to the universality class of the two-dimensional (2D) Ising model [8], however, the finite-size scaling analysis was limited to system sizes up to 6×6 . Here, we use our OSDTWA to simulate the dynamics of the dissipative XYZ model on a square lattice for system sizes between 8×8 and 14×14 , as we describe below.

We consider spin-1/2 particles that interact via anisotropic Heisenberg interactions, whose Hamiltonian has the form

$$H = \sum_{\langle ij \rangle} (J_x \sigma_i^x \sigma_j^x + J_y \sigma_i^y \sigma_j^y + J_z \sigma_i^z \sigma_j^z), \quad (\text{S26})$$

where J_α are the spin-spin couplings between nearest-neighbors, with $\alpha = x, y, z$. Dissipation in the system is realized via spin-flip operators $c_i = \sqrt{\gamma_d} \sigma_i^-$, which have the same form as in the dissipative Ising model considered in the main text. If J_x and J_y are anisotropic, i.e., $J_x \neq J_y$, the system can undergo a dissipative phase transition from a paramagnetic state with zero magnetization in the xy plane to a ferromagnetic state with nonzero magnetization in the xy plane [7].

We implement the OSDTWA following the description provided in the previous section. In particular, we generate the initial states according to the DTWA, i.e., we fix $S_i^z = -1$ and randomly choose $S_i^x, S_i^y = \pm 1$ with equal probability. For the time evolution we evolve the initial state under the effective Hamiltonian based on Eq. (S14). This results in

the equations of motion

$$\dot{S}_i^x = -2S_i^y \sum_j J_z S_j^z + 2S_i^z \sum_j J_y S_j^y - \frac{\gamma_d}{2} S_i^x, \quad (\text{S27})$$

$$\dot{S}_i^y = 2S_i^x \sum_j J_z S_j^z - 2S_i^z \sum_j J_x S_j^x - \frac{\gamma_d}{2} S_i^y, \quad (\text{S28})$$

$$\dot{S}_i^z = -2S_i^x \sum_j J_y S_j^y + 2S_i^y \sum_j J_x S_j^x - \frac{\gamma_d}{2} (S_i^z + S_i^0), \quad (\text{S29})$$

$$\dot{S}_i^0 = -\frac{\gamma_d}{2} (S_i^z + S_i^0), \quad (\text{S30})$$

where the index j runs over nearest neighbors corresponding to the site i . Again, we numerically solve these equations of motion with a fourth-order Runge Kutta method. The time evolution undergoes random quantum jumps, which are implemented following the Monte-Carlo procedure described above. To identify the transition, we calculate the steady-state magnetization defined as

$$m = \langle (m_x^2 + m_y^2)^{1/2} \rangle, \quad \text{with} \quad m_\alpha = \frac{1}{N} \sum_i^N S_i^\alpha, \quad (\text{S31})$$

where $\langle \dots \rangle$ represents the trajectory average and N is the total number of lattice sites. For our analysis, we choose $J_x/\gamma_d = 0.9$ and $J_z/\gamma_d = 1$, and vary J_y/γ_d to determine the transition. We use the integration time step $\gamma_d \Delta t = 0.005$ and a maximum time of $\gamma_d t = 3000$, for which the time evolution of $m(t)$ reaches a well-defined steady state. In Fig. S4(a), we show the OSDTWA steady-state value of the magnetization for various system sizes between 8×8 and 14×14 . Increasing J_y triggers a phase transition between a paramagnet having zero and a ferromagnet having nonzero magnetization, respectively.

To capture the precise nature of the transition we use the finite-size scaling behavior

$$m(J_y, L) = L^{-\beta/\nu} \bar{m}((J_y - J_{y,c})L^{1/\nu}), \quad (\text{S32})$$

where β and ν are the critical exponents, L is the linear dimension of the system, and $J_{y,c}$ is the location of the critical point [11]. We follow the scaling behavior based on Eq. (S32) and therefore scale the magnitude as $mL^{\beta/\nu}$, where we use the previously suggested values $\beta = 1/8$ and $\nu = 1$ of the two-dimensional Ising model [8], see Fig. S4(b). The different system size results cross at $J_y = J_{y,c} \approx 1.0431 \pm 0.0002$, which we identify as the critical point. Error bars can be estimated from the standard deviation $\Delta m = (\langle m^2 \rangle - \langle m \rangle^2)^{1/2}$, resulting in an error of $\Delta m / \sqrt{N_t - 1}$, where N_t is the number of trajectories. We note that this prediction for the critical point is in good agreement with both the cluster mean-field analysis ($J_{y,c} = 1.03$) [10] and the tree tensor network approach ($J_{y,c} = 1.07 \pm 0.02$) [8].

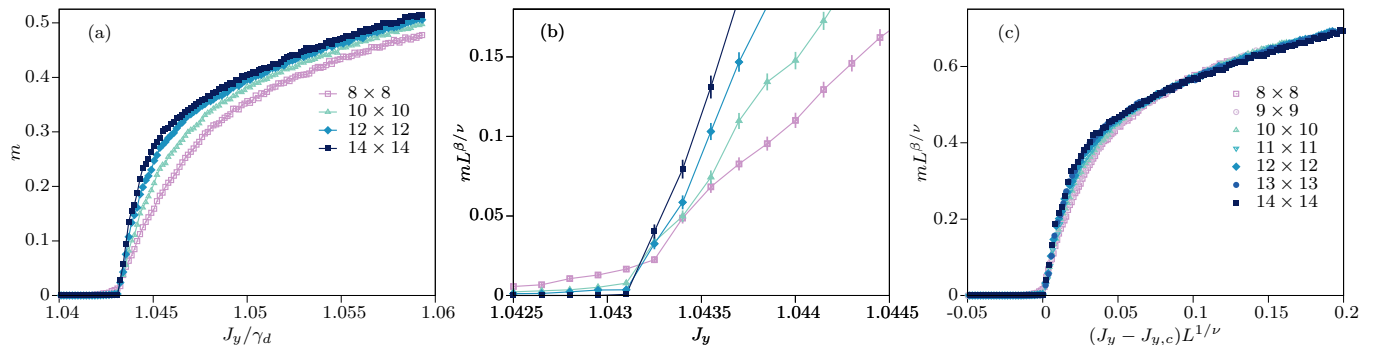


FIG. S4. Critical behavior of the dissipative XYZ model. (a) Magnetization m as a function of J_y/γ_d for varying system sizes between 8×8 and 14×14 . We use $J_x/\gamma_d = 0.9$ and $J_z/\gamma_d = 1$. Results were obtained using trajectory numbers between 600 and 1,000. (b) Scaled magnetization $mL^{\beta/\nu}$ with $\beta = 1/8$ and $\nu = 1$ according to the 2D Ising universality class. Using a linear interpolation between the data points, all curves cross around $J_y = J_{y,c} \approx 1.0431 \pm 0.0002$, with the error being given by the spacing between the data points. Error bars on the individual curves were obtained from the statistical sampling error; see text. (c) $mL^{\beta/\nu}$ versus $(J_y - J_{y,c})L^{1/\nu}$ shows a data collapse for all system sizes, confirming the transition belonging to the 2D Ising universality class.

In Fig. S4(c), we plot $mL^{\beta/\nu}$ versus $(J_y - J_{y,c})L^{1/\nu}$, which results in all data collapsing onto a single curve, i.e., we have used the correct critical exponents to describe the phase transition, confirming the transition belonging to the universality class of the two-dimensional Ising model.

-
- [1] A. J. Daley, Quantum trajectories and open many-body quantum systems, *Adv. Phys.* **63**, 77 (2014).
 - [2] J. Dalibard, Y. Castin, and K. Mølmer, Wave-function approach to dissipative processes in quantum optics, *Phys. Rev. Lett.* **68**, 580 (1992).
 - [3] R. Dum, P. Zoller, and H. Ritsch, Monte Carlo simulation of the atomic master equation for spontaneous emission, *Phys. Rev. A* **45**, 4879 (1992).
 - [4] R. Dum, A. S. Parkins, P. Zoller, and C. W. Gardiner, Monte Carlo simulation of master equations in quantum optics for vacuum, thermal, and squeezed reservoirs, *Phys. Rev. A* **46**, 4382 (1992).
 - [5] H.-P. Breuer and F. Petruccione, *The Theory of Open Quantum Systems* (Oxford University Press, Oxford, 2002).
 - [6] W. H. Press, S. A. Teukolsky, and W. T. Vetterling, *Numerical Recipes in C* (Cambridge University Press, Cambridge, 1992).
 - [7] T. E. Lee, S. Gopalakrishnan, and M. D. Lukin, Unconventional Magnetism via Optical Pumping of Interacting Spin Systems, *Phys. Rev. Lett.* **110**, 257204 (2013).
 - [8] R. Rota, F. Storme, N. Bartolo, R. Fazio, and C. Ciuti, Critical behavior of dissipative two-dimensional spin lattices, *Phys. Rev. B* **95**, 134431 (2017).
 - [9] A. Kshetrimayum, H. Weimer, and R. Orús, A simple tensor network algorithm for two-dimensional steady states, *Nature Commun.* **8**, 1291 (2017).
 - [10] J. Jin, A. Biella, O. Viyuela, L. Mazza, J. Keeling, R. Fazio, and D. Rossini, Cluster Mean-Field Approach to the Steady-State Phase Diagram of Dissipative Spin Systems, *Phys. Rev. X* **6**, 031011 (2016).
 - [11] J. L. Cardy, *Scaling and Renormalization in Statistical Physics* (Cambridge University Press, Cambridge, 1996).